Cytosolic N- and C-Termini of the *Aspergillus nidulans* FurE Transporter Contain Distinct Elements that Regulate by Long-Range Effects Function and Specificity

Georgia F. Papadaki [1], George Lambrinidis [2], Andreas Zamanos [1], Emmanuel Mikros [2] and George Diallinas [1]

1 - Department of Biology, *National and Kapodistrian University of Athens, Panepistimioupolis, Athens 15784, Greece*
2 - Department of Pharmacy, *National and Kapodistrian University of Athens, Panepistimioupolis, Athens 15771, Greece*

Correspondence to Emmanuel Mikros and George Diallinas: *mikros@pharm.uoa.gr, five]diallina@biol.uoa.gr.*
https://doi.org/10.1016/j.jmb.2019.07.013
Edited by I B. Holland

Abstract

FurE, a member of the NCS1 family, is an *Aspergillus nidulans* transporter specific for uracil, allantoin and uric acid. Recently, we showed that C- or N-terminally truncated FurE versions are blocked for endocytosis and surprisingly show modified substrate specificities. Bifluorescence complementation assays and genetic analyses supported the idea that C- and N-termini interact dynamically and through this interaction regulate selective substrate translocation. Here we functionally dissect and define distinct motifs crucial for endocytosis, transport activity, substrate specificity and folding, in both cytosolic termini of FurE. Subsequently, we obtain novel genetic and *in silico* evidence indicating that the molecular dynamics of specific N- and C-terminal regions exert long-range effects on the gating mechanism responsible for substrate selection, via pH-dependent interactions with other internal cytosolic loops and membrane lipids. Our work shows that expanded cytoplasmic termini, acquired through evolution mostly in eukaryotic transporters, provide novel specific functional roles.

Introduction

Transporters are membrane proteins that mediate cellular import and export of nutrients, metabolites, signaling molecules or drugs, and are thus essential for cell communication and life. Despite their evolutionary, structural and functional differences, all transporters appear to use an alternating-access mechanism where a substrate binding site, in "allosteric" cooperation with distinct gating domains, alternates between multiple conformations for receiving and delivering specific substrate(s) from one side of the membrane to the other. This basic mechanism, carried out by dynamic movements of the main transmembrane body and assisted by the flexibility of interconnecting hydrophilic loops, exists in different forms, of the so-called the rocker-switch, the rocking-bundle or the elevator sliding mechanisms [10,25,28,33].

One of the best-studied families of transporters due to a plethora of genetic and biochemical findings concerning fungal members of the family [35,37,55] is the nucleobase cation symporter 1 (NCS1) family. This, together with extensive structural, biophysical and functional data relating to bacterial homologs, principally the benzyl-hydantoin/Na^+ Mhp1 symporter [61],[53],[54] and the allantoin/H^+ PucI symporter [41]. Based on crystal structures of Mhp1, NCS1 proteins consist of 12 transmembrane α-helical segments (TMSs) interconnected with rather short loops and cytosolic N- and C-termini. TMSs 1–10 are arranged as a five-helix intertwined inverted repeat (5HIRT), the LeuT-fold, also found in other transporter families involved in neurotransmitter, sugar, amino acid and drug transport [10,52,59,62]. The last two TMSs (11 and 12) appear crucial for the oligomerization state of some NCS1-like transporters, rather

than being involved in the mechanism of transport [22].

The crystal structures available for Mhp1 correspond to conformational distinct outward-facing open, substrate-occluded and cytoplasm-open topologies [53,54,61], indicative of an alternating access rocking-bundle transport mechanism [2,12,29,54]. In all cases, TMSs 1, 2, 6, and 7 form a four-helix bundle, while TMSs 3, 4, 8, and 9 form a "hash sign" motif. The substrate and Na^+ binding sites are found between the hash and bundle motifs and involve residues in TMSs 1 and 6, at helical break-point positions. Ligand binding to the outward-facing conformation causes TMS10, the outer gate, to bend and occlude the binding site. Gate closure elicits a transition to the inward-facing conformation by the movement of the hash domain relative to the bundle domain. The main body movements lead subsequently to opening of an inner gate and release of Na^+ and substrate [6,29,54]. Importantly, structural studies on Mhp1 have been found to be in excellent agreement with functional studies in two homologous subfamilies of NCS1 present in fungi and plants [35,37,48,55]. In particular, mutations affecting transport kinetics and specificity of members of the Fcy and Fur families have been characterized by crystal structures and modeling approaches to be located both in the substrate binding site and also in the outward-facing gate.

We have recently provided genetic evidence that the turnover, function and intriguingly the specificity of an *Aspergillus nidulans* NCS1 homolog, FurE transporter, depend on interactions of the N- and C-terminal cytoplasmic regions with each other and with the main body of the transporter [46]. We showed that C- or N-terminally-truncated versions of FurE (FurE-ΔC30 or FurE-ΔN21) have increased protein stability in conditions that normally trigger ubiquitylation and endocytic turnover [60]. Interestingly, they lose their capacity to import uric acid, while allantoin and uracil are transported normally.

By isolating genetic suppressors of FurE-ΔC30, which restore uric acid transport, we demonstrated that the deleted part of the C-terminus apparently has a long-distance functional effect on the substrate translocation and gating domains. We also obtained direct genetic evidence using bifluorescence complementation assays that the C-terminus interacts with the distal part of the N-terminus. Our results have suggested that both C- and N-terminal domains are involved in intramolecular dynamics critical for the fine regulation of the mechanism that controls substrate transport [44].

Here, we further dissect the function of the N- and C-terminal domains of FurE and identify distinct linear segments that are crucial for endocytic turnover, transport activity, substrate specificity and folding. By using genetics and molecular dynamics (MD), we provide further evidence that specific residues of the N-terminus interact with residues in internal cytoplasmic loops and the C-terminus in a pH-dependent manner, and via these interactions exert long-range control of the gating mechanism and thus substrate specificity. Our results are discussed within the context of how the evolution of extended termini in eukaryotic transporters has provided new molecular paths for the generation of novel functions.

Results

The N-terminus of FurE is crucial for endocytic turnover, specificity and ER-exit

We previously characterized the function of FurE-ΔN21, a truncated version of FurE lacking the first 21 amino acid residues from its N-terminus, tagged with a GFP epitope. FurE-ΔN21 proved insensitive to signals triggering endocytosis [46]. Interestingly, FurE-ΔN21 has lost its transport capacity specifically for uric acid, but retains normal transport of allantoin or uracil, as judged from relevant growth tests [46] (see also Fig. 1).

Although the truncation in FurE-ΔN21 involved a little conserved segment in Fur homologs, a downstream sequence is absolutely conserved in the Fur subfamily, and also well conserved in several prokaryotic NCS1 homologs, including Mhp1. This sequence contains the motif: **N**-X-D/S-L-X-**P** (Fig. 1A). The first Asn and the last Pro are absolutely conserved in all NCS1 members, whereas the D-L sequence is present in fungal Fur homologs, but replaced by S-N/Q in Mhp1 and with various substrate specificities in some other prokaryotic members. Given its presence in prokaryotic NCS1 transporters, we predicted that this N-terminal cytosolic motif might be important for the structure and/or function of this group of transporters, rather than for membrane traffic, endocytosis or other eukaryotic-specific function. We named this motif, the *L*oop *I*nteracting *D*omain (LID) motif, in accordance with a previous publication [30], and for reasons that will become apparent later.

To investigate the function of the LID segment (residues 21–29) and relate this to the already established role of the distal part of the N-terminus (residues 1–21) in endocytosis and substrate specificity, we constructed and analyzed two new truncated FurE versions. The first deleted the entire N-terminus (FurE-ΔN38), for LID, and the second for the first 11 amino acid residues (FurE-ΔN11).

FurE-ΔN38 was retained in the ER membrane and consequently had no apparent transport activity (Fig. 1B, C). In contrast, as judged by growth tests, FurE-ΔN11 possessed normal apparent transport activity and substrate specificity

and, when compared to wild-type FurE and FurE-ΔN21 (Fig. 1B, C), showed partial resistance to endocytic internalization. Comparing the effects of the three truncated versions (FurE-ΔN11, FurE-ΔN21 and FurE-ΔN38), it seemed that the distal 10 residues of the N-terminus contribute to endocytosis but not critical for transport activity or specificity, whereas residues within segment 11–20 contribute to endocytosis and are crucial for substrate specificity (compare truncations ΔN11 to ΔN21 in respect to endocytosis and growth on uric acid) (Fig. 1B, C). Finally, segments 21–37 proved critical for ER-exit (compare truncations ΔN21 to ΔN38 in respect to subcellular localization). This analysis was insufficient to define the role of the LID, as ΔN38 deletion was not sorted to the PM.

The LID motif determines substrate specificity but is dispensable for PM localization, transport activity or endocytic turnover

We systemically tested the function of the LID segment, present in the middle part of the N-terminus (residues 21–29), by Ala substitutions of its conserved residues (N24A, D26A, D26A/L27A and P29A). Figure 2A shows that LID mutations allow FurE-mediated growth on uric acid and allantoin and confer sensitivity to 5-fluorouracil (5FU), similar to that of an isogenic strain expressing wild-type FurE. Surprisingly, mutations N24A, D26A and especially D26A/L27A resulted in reduced minimal growth on xanthine, which normally does not support any xanthine-dependent growth by FurE.

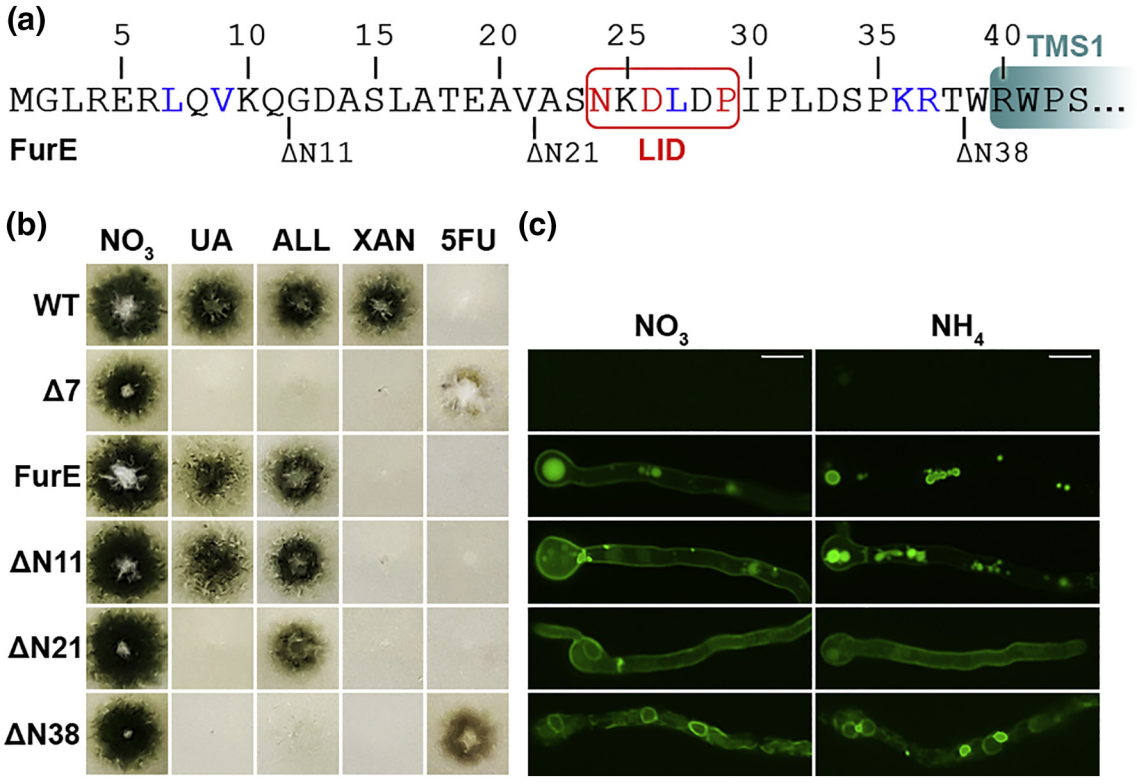

Fig. 1. The N-terminus of FurE is crucial for endocytic turnover, specificity and ER-exit. (A) Schematic representation of the cytosolic N-terminal region of FurE depicting the limits of deletions ΔN11, ΔN21 and ΔN38, and the conserved LID motif (boxed in red). Conserved amino acids in *Aspergilli* and in all fungal homologs are marked in blue and red, respectively. (B) Growth test analysis of a standard wild-type (WT) *A. nidulans* strain, a Δ7 strain lacking all genes encoding nucleobase related transporters [45] (*uapAΔ uapCΔ azgAΔ furDΔ furAΔ fcyBΔ cntAΔ*), and isogenic Δ7 transformants expressing functional GFP-tagged ΔN11, ΔN21, ΔN38 and wild-type FurE versions from the strong *gpdA* promoter. The Δ7 strain has an intact endogenous FurE gene transporter, but this is very little expressed under standard conditions and thus does not contribute to detectable transport of its physiological substrates (UA, ALL) or to sensitivity in 5FU [37]. The test was performed on minimal media (MM) containing nitrate (NO_3^-), uric acid (UA), allantoin (ALL), xanthine (XAN) as sole nitrogen sources, and NO_3 plus the toxic nucleobase analogue 5FU, at 37 °C and pH 6.8. (C) *In vivo* epifluorescence microscopy of the same strains grown until the stage of young hyphae (16–18 h in MM plus NO_3^-). In the right panel, ammonium tartrate (NH_4^+) was added 2 h before microscopic observation. NH_4^+-elicited endocytosis is visible as reduced fluorescent signal from the cell periphery concomitant with the appearance of cytosolic structures, which correspond to vacuoles and endosomes [37,46]. For more details, see Materials and Methods. Scale bars represent 5 μm.

In other words, Ala substitutions seem not to affect the capacity for transport, but replacements of N24, D26 and especially D26/L27 enlarged the range of substrate specificity to include xanthine. Figure 2B confirmed that none of the mutations affect stable localization of FurE into the PM (upper panel), and none has an effect on the sensitivity of FurE to endocytosis elicited by NH_4^+ (lower panel).

We performed direct uptake assays to further understand the effect of LID mutations in FurE transport mechanism by measuring radiolabeled uracil accumulation, a low-affinity substrate of FurE [37]. Radiolabeled uracil was used as radiolabeled allantoin is not available commercially and radiolabeled uric acid is very unstable. Radiolabeled uracil accumulation in FurE mutants is similar (D26A) or ~2- to 2.5-fold higher (N24A, D26A/L27A, P29A) to the wild-type FurE (Fig. 2C, gray bars). This not only explains sensitivity to 5FU but also is consistent with normal growth on allantoin or uric acid (Fig. 2A).

Given that mutants N24A, D26A and D26A/L27A also reduced growth on xanthine, we also tested whether this was due to an increase in the affinity for xanthine. Note that wild-type FurE has practically no affinity for xanthine; that is, $K_i > 1$ mM, [37]. To measure xanthine binding, we performed standard competitive inhibition assays that measure radiolabeled uracil accumulation in the presence of excess xanthine (1 mM), as described before [36]. Our results show that FurE single mutants N24A, D26A and P29A have no significant xanthine binding, similarly to wild-type FurE. In contrast, in the double

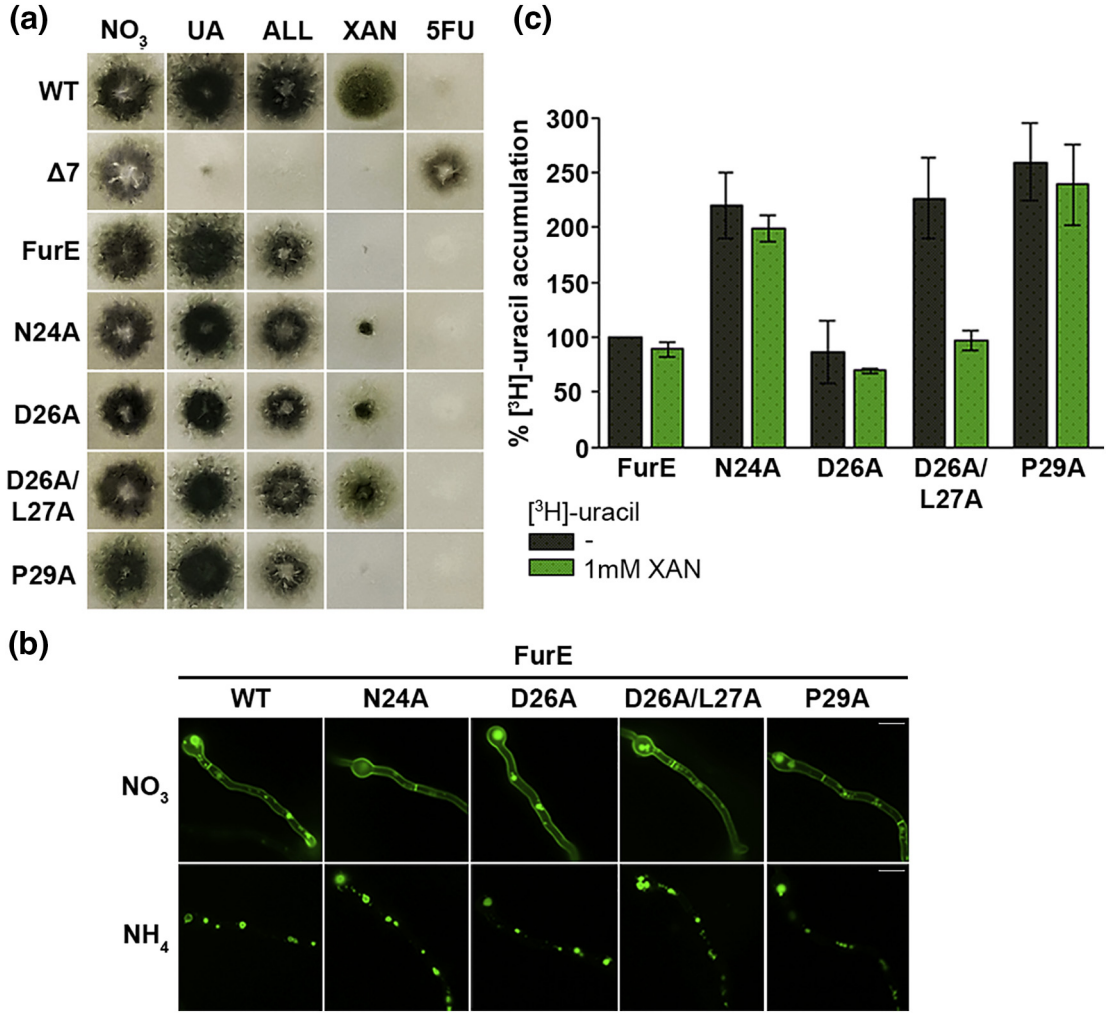

Fig. 2. The LID motif of FurE is crucial for substrate specificity, but dispensable for PM localization, transport activity and endocytic turnover. (A) Growth tests of the control strains (WT, Δ7, FurE) and strains expressing GFP-tagged FurE mutations in the LID (N24A, D26A, D26A/L27A, P29A). Details are as in Fig. 1B. (B) Subcellular localization of the FurE mutants. Noticeably, none of the LID mutations affect the PM localization of FurE (NO_3^- panel) or its endocytosis elicited by NH_4^+. Details are as in Fig. 1C. Scale bars represent 5 μm. (C) Comparative [^{3}H]-uracil (0.5 μM) accumulation and competition assays in the presence of excess (1 mM) of xanthine in strains expressing wild-type FurE, FurE-N24A, FurE-D26A, FurE-D26A/L27A or FurE-P29A. Results shown are averages of three independent assays. Standard deviation is depicted with error bars.

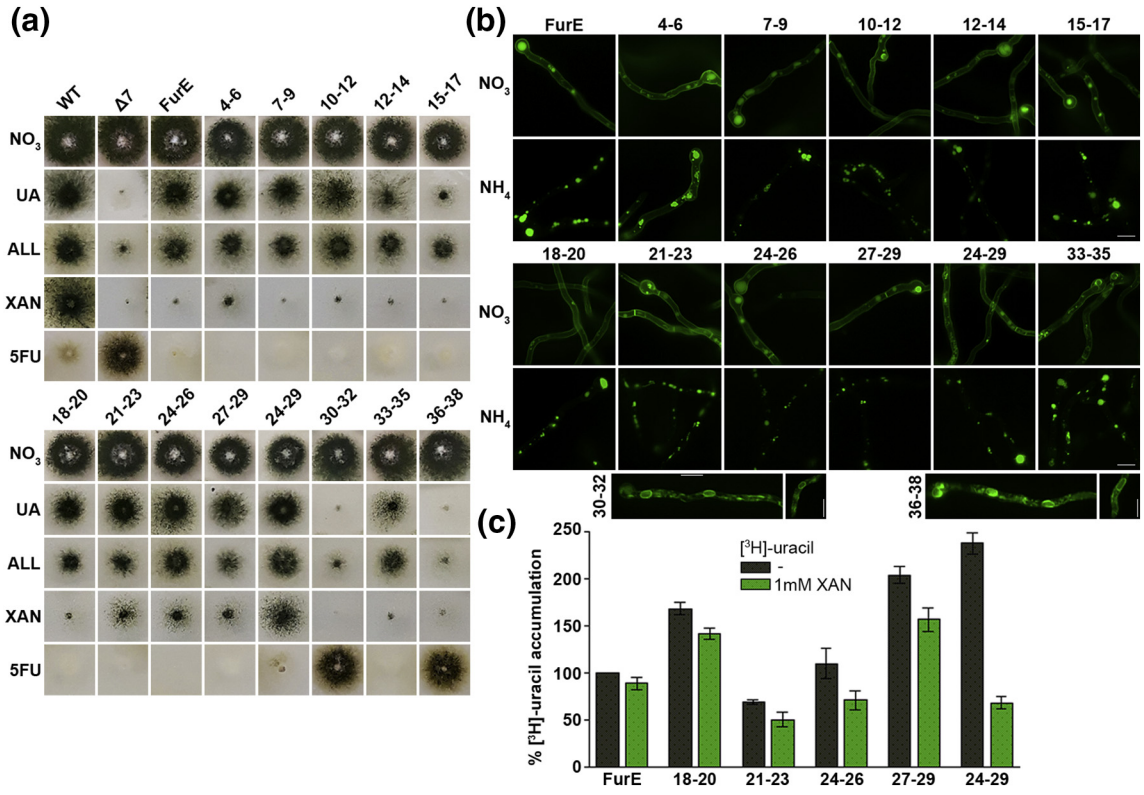

Fig. 3. Delimitation of the N-terminal segments crucial for endocytosis, substrate specificity or ER-exit. (A) Growth tests of control strains and FurE mutants expressing triple Ala substitutions in the FurE N-terminus. Each mutant is named after the position of residues replaced. Notice that mutant 15–17 has significantly reduced capacity to grow on UA, whereas mutants 21–23, 24–26, 27–29 and mostly 24–29 gained the ability to grow on XAN. Details are as in Fig. 1B. (B) Epifluorescence microscopy of the mutants shown in panel A. In the presence of NO_3^- (upper panel), most mutants showed normal PM localization of FurE except mutant 7–9, which showed a degree of instability and increased vacuolar turnover, and mutants 30–32 and 36–38 where FurE was blocked in perinuclear ER rings [46]. Also, all mutants except 4–6 showed the same degree of endocytic turnover as the wild-type FurE after addition of NH_4^+. Mutant 4–6 seems to be partially insensitive to endocytosis, marking the PM even in the presence of NH_4^+. Details are as in Fig. 1C. Scale bars represent 5 μm. (C) Uptake assays measuring accumulation and competition assays by excess substrate of the different strains carrying triple mutations. Details are as in Fig. 2C. Standard deviation is depicted with error bars.

mutant D26A/L27A, uracil uptake was inhibited to >50% by xanthine (Fig. 2C, green bars).

Despite an increase in xanthine binding in the double mutant, FurE-mediated reduced growth, as judged by the single mutants, might not be assigned solely to an increase in xanthine affinity. The growth behavior and transport kinetics of the single mutants, and to a certain degree of the double mutant, are also characteristics of mutations modifying the gating mechanism in other transporters [9,47]. Overall, our results suggested that the LID sequence is critical for specificity by altering the mechanism of gating, rather than by modifying significantly substrate interactions in the bona fide substrate binding site.

Notably, while Ala replacements of N24 and D26/L27 enlarged the specificity range of substrates transported by FurE (allantoin, uracil, uric acid *and* xanthine), deletion of N-terminal residues 1–21 led to restriction of the substrates transported (uracil and allantoin), as described here and previously [46]. A similar restriction of substrates has also been observed by deleting the last 30 amino acid residues of the C-terminus [46]. These observations will be explained later, in context.

Delimitation of N-terminal segments crucial for endocytosis, substrate specificity or ER-exit

To obtain a deeper view on the amino acid residues that are crucial for endocytosis *versus* those that are important for substrate specificity or ER-exit, we systematically mutated, by triple Ala substitutions, the entire N-terminus of FurE. Our results are summarized in Fig. 3. Growth tests on purines, as N sources, or on toxic nucleobase analogues, revealed that the only triple mutations that led to loss of apparent FurE-mediated transport, as judged by lack of growth on allantoin, or uric acid and resistance to 5FU, are those affecting residues

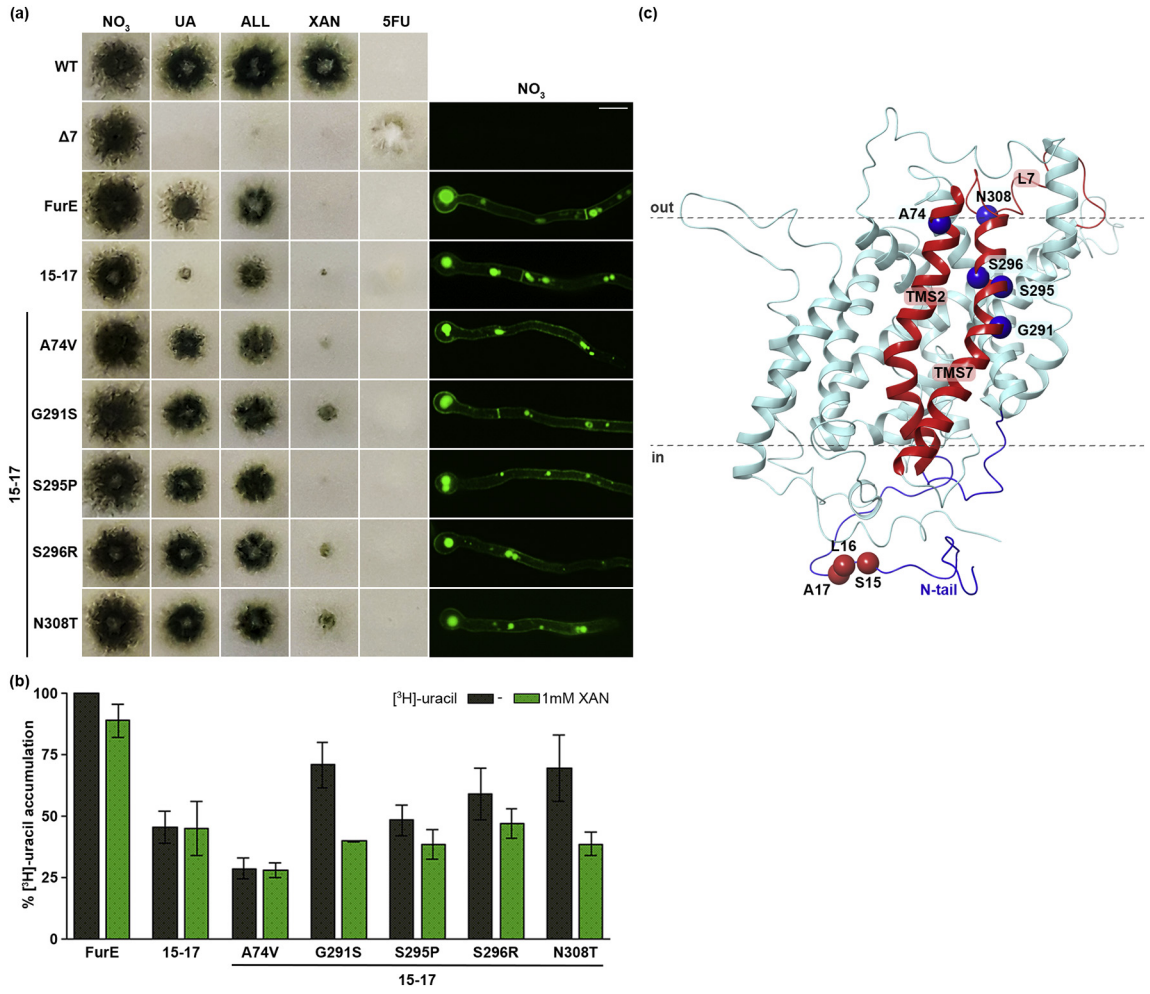

Fig. 4. Genetic evidence for a long-distance effect of the N-terminus on the function of the substrate translocation trajectory. (A) Growth tests (left panel) and subcellular localization (right panel) of the control strains and FurE-S15A/L16A mutant (named 15–17 in the figure) and its suppressor strains. Notice that all suppressors are normally localized in the PM and all have regained the ability of wild-type, FurE-mediated, growth on UA. Details are as in Fig. 1B and C. Scale bar represents 5 μm. (B) Relative accumulation of radiolabeled uracil and competition assays in the presence of excess substrate in different suppressors. Details are as in Fig. 2C. Standard deviation is depicted with error bars. (C) Topology of the suppressor mutations (blue spheres) compared to the original N-terminal S15A/L16A mutation (red spheres).

30–32 and 36–38 (Fig. 3A). This was confirmed by epifluorescence microscopy, which showed that these two mutations led to retention of FurE in the ER membrane, while similarly to wild-type FurE, all other mutant versions of FurE were properly located in the PM and in some vacuoles (Fig. 3B, see NO_3^- panels). Very minor reduction of growth on allantoin, compared to wild-type FurE, was observed in Ala mutations affecting residues 27–29, but this mutant was still highly sensitive to 5FU, suggesting that its transport activity was generally not affected (Fig. 3A). Notably, the triple mutations concerning residues 21–23, 24–26, 27–29 and mostly the hexavalent Ala substitution 24–29 conferred growth on xanthine, which was not seen in the control strain lacking FurE (Δ7) or to that expressing a wild-type FurE (Fig. 3A). This suggests that not only N24 and D26 but also residues 24–29 of the LID are critical for substrate specificity. In addition, growth on uric acid was reduced progressively in mutations affecting residues 10–12, 12–14 and mostly 15–17, and also moderately in mutant 33–35 (Fig. 3A). This means that segments neighboring the LID contribute differentially to substrate selection.

Given that several of the N-terminal triple Ala substitutions conferred growth on xanthine, we tested whether this is due to an increase in the binding affinity for xanthine or is due to a modification in selective gating. We measured accumulation or competition by excess xanthine of radiolabeled uracil in mutants 18–20, 21–23, 24–26, 27–29 and 24–29 (Fig. 3C). Accumulation of radiolabeled uracil was significantly reduced in 27–29 and 24–29 (~20%–25% of wild-type FurE), but little affected or

moderately increased in 21–23, 24–26 or 18–20 (75–160% of wild-type FurE; see gray bars). The effect of mutations on the capacity for uracil uptake was not reflected in differences in growth (e.g., sensitivity to 5FU or growth on allantoin). This is not an anomaly, as reduction in transport capacities that are lower than 70%–75% often does not become apparent in growth tests [9,47]. Estimation of the level of inhibition of radiolabeled uracil accumulation by excess xanthine suggested that the mutations studied do not significantly modify the binding affinity for xanthine, despite a trend toward increased inhibition of uracil uptake, seen mostly obvious in mutant 24–26. Thus, growth on xanthine of FurE mutants seemed not to be due to increased xanthine binding, but rather to an alteration of the gating process, as also suggested previously for the single Ala replacements in the LID region.

We also performed uptake and competition assays in mutant 15–17, which showed reduced uric acid growth. Noticeably, uric acid is the only FurE substrate that is recognized by high affinity (K_m = 20 μM; [37]). However, we could not detect any significant effect of mutation 15–17 on the binding affinity of FurE for uric acid (not shown, suggesting that these mutants affect the process of gating rather than modifying the substrate affinities of Fur.

In terms of sensitivity to endocytosis, the only Ala triplet that led to detectable but moderately reduced internalization was the one affecting residues 4–6 (Fig. 3B, lower panel). This contrasts the total block of endocytosis achieved by deleting residues 1–21 and resembles the partial block by deleting residues 1–11 (see Fig. 1). Noticeably, the distal N-terminal segment of Fur transporter is in general little conserved but seems to contain an excess of positively charged residues, two of which are removed in the Ala mutation replacing residues 4–6. Moreover, given that the interaction of N- and C-termini has also been shown to be critical for endocytosis [46], the deletion of the N-terminal residues 1–21 might well hinder this interaction and thus affect FurE turnover (see also later).

Overall, our results showed that distal residues of the N-terminus are essential for endocytosis, middle N-terminus residues affect specificity, and residues proximal to TMS1 are essential for ER-exit, apparently by affecting proper folding of the transporter.

Genetic evidence for an effect of the N-terminus on the functioning of the substrate translocation trajectory

In order to further understand how the N-terminus might affect substrate specificity, we isolated genetic suppressors of mutant S15A/L16A by directly selecting for revertants re-establishing the capacity for FurE-mediated growth on uric acid. Several mutants were selected after U.V. mutagenesis, and 24 of them were purified and characterized in respect to their growth phenotypes on purines and to amino acid changes that occurred within the FurE ORF. Figure 4A shows that all suppressor mutations characterized, namely, A74V, G291S, S295P, S296R and N308T, confer growth phenotypes on uric acid, allantoin or 5FU similarly to that of the isogenic strain expressing wild-type FurE (left panel), but additionally, all except S295P led to weak but clearly detectable growth on xanthine. Furthermore, none of the suppressors affected the proper localization of FurE in the plasma membrane (right panel).

We also performed radiolabeled uracil uptake or competition assays in mutants A74V, G291S, S295P, S296R and N308T, as previously described. Most of them showed ~50%–70% of wild-type FurE uptake capacity, except A74V which showed 30% transport accumulation (Fig. 4B, gray bars). Importantly, mutants that resulted in reduced growth on xanthine (mostly G291S and N308T) also showed increased binding affinity for xanthine, as indicated by the higher level of competition of uracil accumulation by xanthine compared to wild-type FurE or A74G (Fig. 4B, green bars). This suggests that the specific defect in uric acid transport in the original mutant (15–17), proposed to arise from modification of gating process, might be partially restored by an increase in substrate affinity. All suppressors characterized were localized in the TMS7-L7 segment of FurE and concerned missense substitutions in well-conserved amino acids (Fig. 4C). Notably, this region has been suggested to be critical for gating in Mhp1 [29,54].

FurE modeling supports that the N-terminus interacts with specific cytosolic loops and the C-tail

The next question was how truncations of terminal segments or amino acid substitutions within the cytosolic N- or C-termini [46] might be sensed by the transmembrane part of the transporter that hosts the substrate translocation trajectory and carries out transport. Related to this issue, the homologous Mhp1 crystal structure shows that the 20-amino-acid region proximal to TMS1, which includes the LID, is in an extended conformation that runs parallel to the membrane along all cytoplasmic loops. Based on this observation, Keener and Babst [30] have proposed that in *Saccharomyces cerevisiae* the N-terminus of the homologous Fur4p transporter, and in particular its LID region, might functionally and dynamically interact with several cytoplasmic loops when the transporter acquires an outward-facing conformation. This interaction, being dynamic, might then be disrupted by conformational alteration of the transporter to the inward-facing conformation, elicited by substrate binding. These authors further

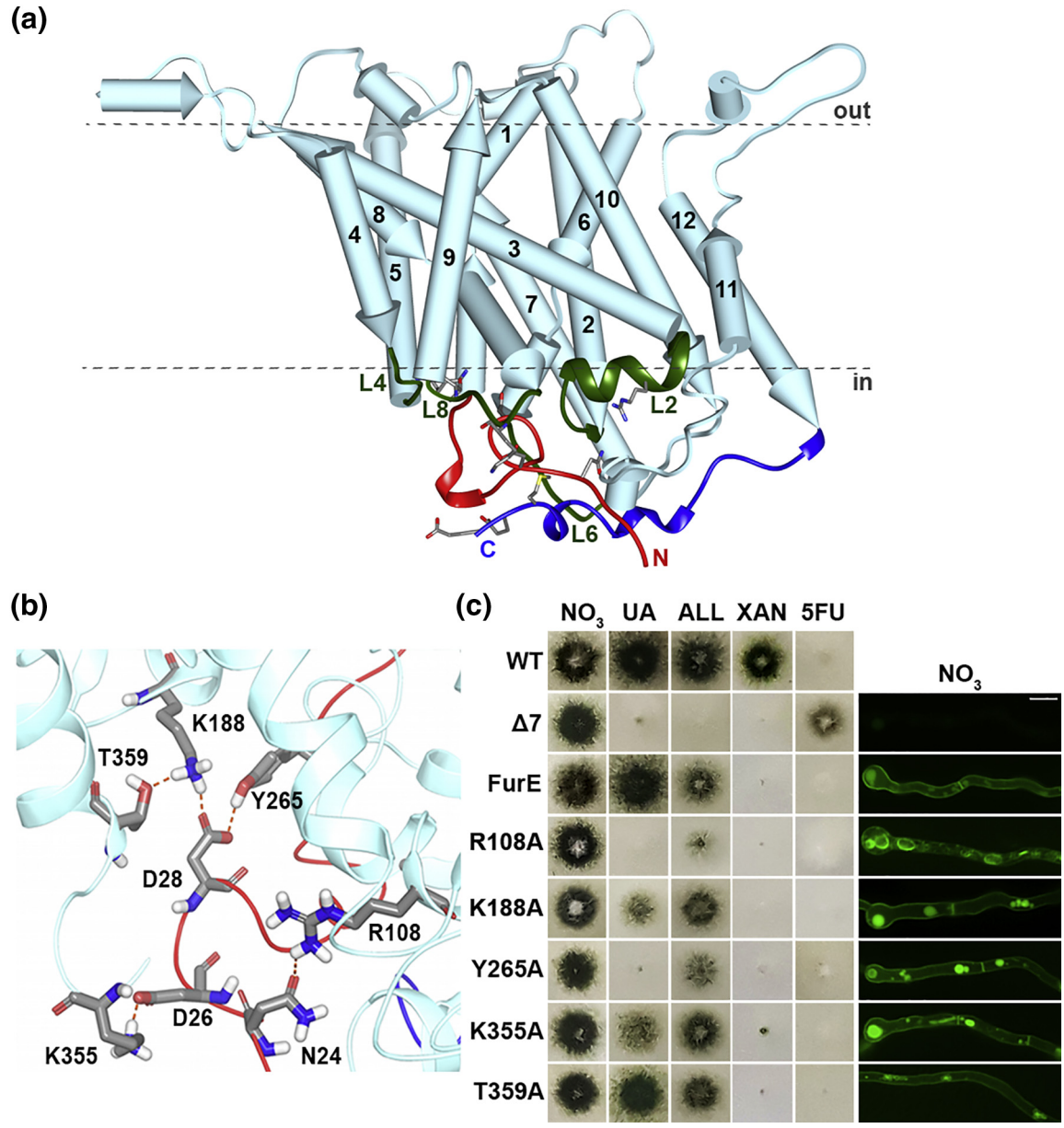

Fig. 5. FurE modeling supports that the N-terminus LID might interact with specific cytosolic loops and the C-tail. (A) FurE model. Notice the close topological distance of the N-terminal region with internal cytosolic loops L2, L4, L6, L8 and the C-tail. (B) Putative major interactions of N-terminal LID with internal cytosolic loops L2, L4 and L8. These interactions were further validated and extended by MD shown in Fig. 7 and Supplementary material. (C) Growth phenotypes (left panel) and subcellular localization (right panel) of loop mutants R108A (L2), K188A (L4), Y265A (L6), K355A and T359A (L8) and control strains. Details are as in previous figures. Notice that all mutant versions of FurE are localized in the PM, except R108A, which is ER-retained. Also, mutations K188A, Y265A and K355A, but not T359A, lead to reduced ability for growth on UA and allantoin, but are still 5FU sensitive, compared to a wild-type FurE. Scale bar represents 5 μm.

proposed that dissociation of the LID from the loops renders the N-terminus accessible for Rsp5/Nedd4-type ubiquitination and degradation, which in turn would explain the phenomenon of transport activity-dependent turnover of Fur4p. They extended this idea to propose that the LID is acting as a conformational-sensitive degron that drives turnover under conditions that lead to partial misfolding of Fur4p. Notably, however, their hypothesis was not supported by targeted mutations in the LID motif, which in their case led to no detectable effect on Fur4p stability or function. Interestingly, Razavi *et al.* [51] very recently also showed that the N-terminus of the mammalian dopamine transporter, which is a

structural homolog of NCS1 transporters, interacts dynamically with specific internal loops and the C-terminus, and thus affects the functioning of dopamine transporter. Based on these reports, we tried to obtain evidence as to whether the LID of FurE interacts with the cytosolic loops of the transporter, and thus affects the dynamics of substrate gating and eventual transport specificity.

To identify possible interactions of the N-terminus with internal loops, we built upon homology and validated via MD a refined FurE structural model. Mhp1 benzylhydantoin permease was used as template in the outward-facing crystal structure (PDB entry 2JLN) according to the alignment presented in Supplementary Fig. 1. Similar to the structure of Mhp1, the model represents a 12 α-helix fold with TMS1–10 divided into two symmetric sets oppositely oriented adopting the 5HIRT motif. The overall three-dimensional structure of the FurE model (Fig. 5A) corresponds to an outward-open conformer, with the transmembrane helices connected with rather short loops except the loop between TMS3 and TMS4 with 21 residues, and the loop separating the core and TMS11–12 is longer (26 residues). The model shows that the side chains of residues critical for transport activity [37], namely, W130 ($W117^{Mhp1}$), Q134 ($Q121^{Mhp1}$) in TMS3, and N341 ($N318^{Mhp1}$) in TMS8, superimpose exactly with the corresponding in Mhp1, oriented to the substrate-binding cavity of the transporter. The residues in TMS1 S54 ($Q42^{Mhp1}$) and S56 ($Ala44^{Mhp1}$), although not conserved, but shown to play a critical role in substrate binding [37], protrude to the binding cavity, and the same holds true for K252, which displays a completely different character from the rest of the NCS1 family members. In most members of the family, this residue has aromatic or aliphatic character (W220 in Mhp1), and further studies are needed to fully elucidate the function of this variant [37]. Other residues common to all members of the NCS1 family are W48 (TMS1), which is not oriented toward the translocation pathway, and R108 in L2, which interacts with H427 in L10 and the backbone carbonyl group of L420 in the same loop. R108 is positioned in a hydrophobic crevice between TMS3 and TMS8, which is closed by the LID residues 22–30. A number of specific and putative dynamic contacts of the residues of the N-terminus, and particularly of the LID region, with residues of internal loops and the C-terminus are summarized in Supplementary Table 1, the most important of which are depicted in Fig. 5B. The main interactions identified are as follows: N24 (LID) with R108 (L2), D26 (LID) with K355 (L8), D28 (LID) with K188 (L4) and Y265 (L6). In addition, K188 in L4 seems to interact with L8 (T359). Residues 32–39 of the N-terminus may also contact several residues in L2, L6 and L8 and specific residues of the C-tail, such as M505, and probably E506 and E507. Overall, the LID residues 24–29 are predicted to interact with L2, L4, L6 and L8, while its downstream region (residues 32–39), proximal to TMS1, interacts with L2, L4, L6 and the C-terminus. The C-terminus itself might additionally interact with the FurE core domain, mostly via salt bridges of E497 and E506 with R418 (L10) and R270 (L6). These interactions were further validated by more extensive MD (see later). Noticeably, despite the low similarity of FurE and Mhp1, similar interactions between the N-terminus and L2, L6, L8 and L10 and the C-terminus are also observed in Mhp1 (Supplementary Table 1). It is worth noting that in the case of the outward open conformation of LeuT, the N-terminal $R5^{LeuT}$ interacts with $D369^{LeuT}$ in TMS8 forming a salt bridge, which is disrupted in the inward conformation, as TMS1a and TMS8 move apart [34].

Assuming the above proposed interactions occur, specific mutations in specific loop residues that interact with termini might also affect specificity. To validate experimentally this assumption and the proposed LID-loops interactions, we constructed and functionally analyzed the following loop mutations; R108A in L2, K188R in L4, Y265A in L6, K355A and T359A in L8. Figure 5C shows the growth phenotypes and subcellular localization of the corresponding FurE mutants. Mutation R108A resulted in total ER-retention and thus apparently caused significant FurE misfolding. Thus, no rigorous conclusion on the role of R108 in specificity could be drawn. All other mutants were normally localized in the PM and retained at least an apparent normal capacity to transport 5FU. Y265A resulted in reduced allantoin and no uric acid transport, while mutants K188A and K355A had significantly reduced ability to transport uric acid. Finally, T359A showed wild-type transport level for both substrates. In other words, K188 (L4), Y265 (L6) and K355 (L8) were crucial for determining the specificity profile of FurE. Noticeably, while mutations within the LID (residues 24–29) enlarged the specificity range of substrates to include xanthine, mutations in loops L2, L6 or L8 restricted the set of substrates to mostly 5FU and allantoin, similarly to mutations present just proximal to the LID (residues 12–17). These findings suggest that N-terminus/LID interactions with other internal loops are complex, and thus, the actual outcome in respect to fine changes in specificity of different Ala substitutions is difficult to predict a priori.

The LID is crucial for determining pH-dependent specificity of FurE

Given that FurE is a proton symporter [37], we also tested whether its function, and specifically that of the LID motif, might be differentially affected by the proton or cation gradient of the membrane. We tested FurE-mediated growth phenotypes on relevant substrates or toxic analogues in different pHs, as well as in the presence of a strong Na^+ gradient. The presence of Na^+ gradient was found not to affect the apparent function of wild-type or mutant FurE. Contrastingly, we observed a notable

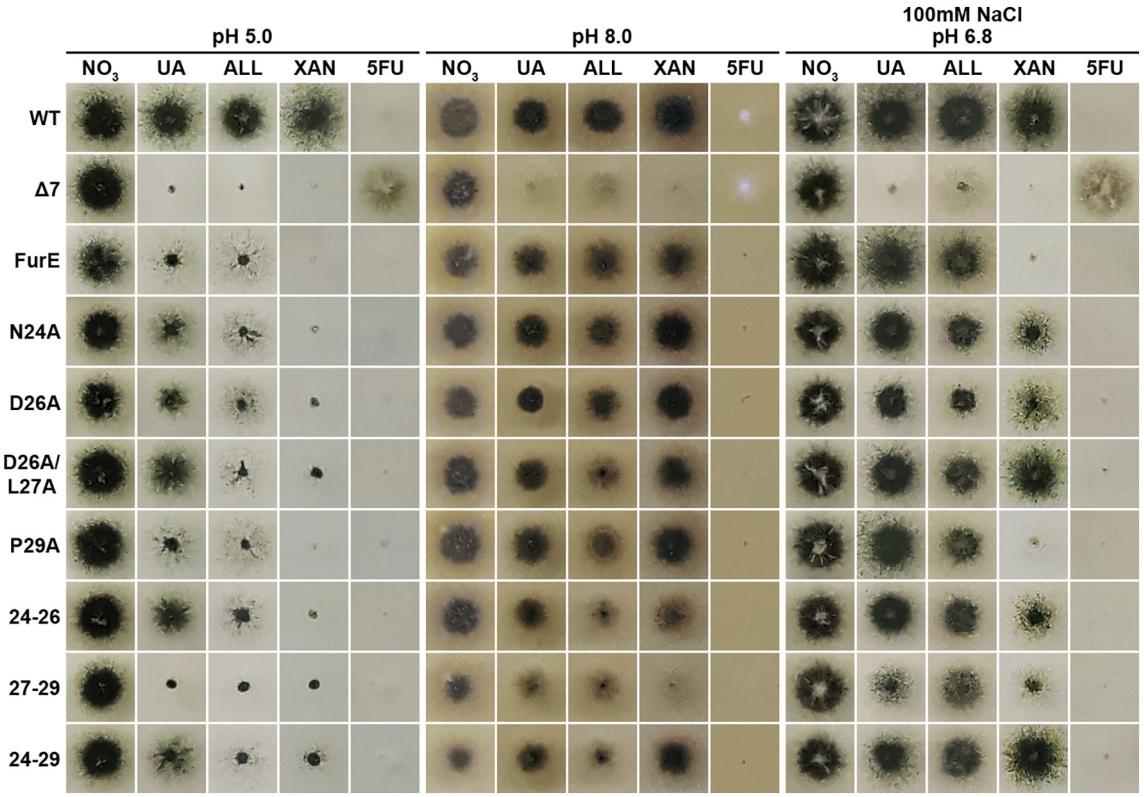

Fig. 6. pH dependence of specificity mutations suggest that ion coupling affects LID interactions and gating. Growth tests of control strains and LID mutations in pH 5.0, 8.0 and 6.8 but in the presence of high Na^+ gradient. For details, see Materials and Methods.

pH-dependence of FurE activity, reflected in growth phenotypes, as highlighted in Fig. 6. In particular, wild-type FurE had significantly reduced apparent transport activity at pH 5.0, as judged by the reduced growth on uric acid and allantoin of the relevant strain, which, however, could still efficiently transport uracil, reflected sensitivity to 5FU. This contrasts the growth phenotypes observed at pH 6.8, the standard pH where *A. nidulans* is tested (see previous figures). At pH 8.0, FurE confers normal growth on uric acid and allantoin, as well as 5FU sensitivity, but unexpectedly, also leads to significant growth on xanthine, which is not a substrate at pH 6.8 or 5.0 (Fig. 6, middle panel). Thus, the overall picture is that FurE has a previously unnoticed pH-dependent substrate profile. At low pH, FurE efficiently transports solely 5FU (and apparently uracil); at neutral pH, FurE also transports uric acid and allantoin; and at pH 8, FurE additionally transports xanthine.

The FurE LID mutants also showed distinct pH-dependent phenotypes. At pH 5.0, most LID mutants (N24A, D26A, D26A/L27A, 24–26 and to a lower degree P29A) grow well on uric acid, unlike the strain expressing the wild-type FurE, while their ability to grow on allantoin or uracil remained similar to that of the wild-type FurE. In other words, at low pH, LID mutants regain wild-type transport capacity for uric acid, but not for allantoin. At pH 8.0, these mutants conserved the wild-type FurE capacity for xanthine transport, which was also apparent at pH 6.8. These findings revealed that at low pH, wild-type FurE functions as a highly specific 5FU (uracil) transporter, incapable for transporting other structurally related substrates, whereas at basic pH, FurE becomes an efficient broad-specificity promiscuous transporter, translocating 5FU, uric acid, allantoin and xanthine.

Given that LID mutations showed a distinct pH behavior compared to wild-type FurE, our results suggested that the protonation state of specific residues in the LID, especially the polar or charged residues N24, D26 or D28, might be responsible for the pH-dependent differences in substrate specificity. Most importantly, Ala mutations in the LID mimic the effect of basic pH, leading to increased promiscuity (i.e., acquisition of the ability to transport xanthine). This observation is discussed further later.

pH-dependent interactions of the LID with intracellular loops affect gating

In order to gain better insight of the interactions between LID and intracellular facing loops, a more detailed structural study was undertaken by running specific MD calculations that would provide

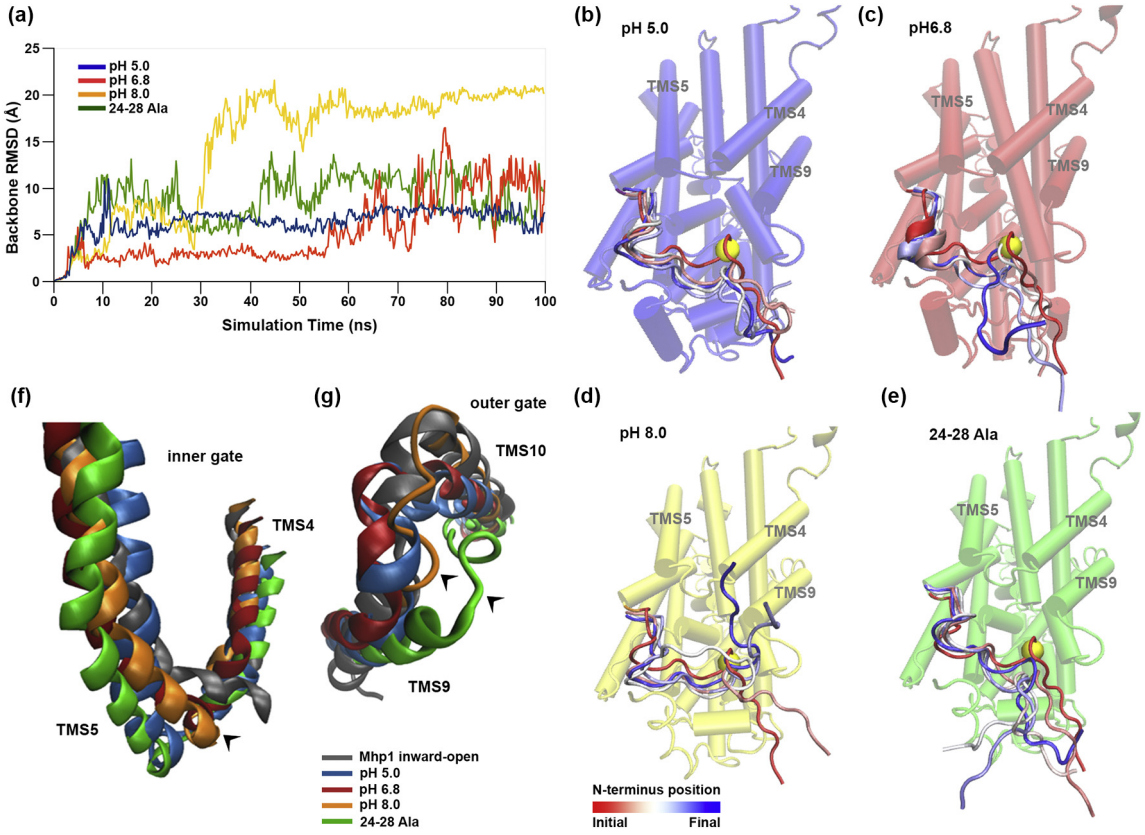

Fig. 7. MD of FurE at different pHs and in the LID mutant (A) RMSD of all Ca atoms of the LID residues 20–40 in respect to the initial structure (blue, pH 5.0; red, pH 6.8; yellow, pH 8; and green, 24–28 Ala mutant). (B–E) Schematic representation of FurE cytoplasmic view together with the conformational transition of the LID residues. Snapshots were taken every 25 ns along the transition pathway and are illustrated color code (red for the initial and blue for the final position). Proline 29 showing the residue of the LID most flexible part is labeled as a yellow sphere. (F–G) Comparison of the Mhp1 crystal structure (gray) in the inward-open form (PDB 2x79) with the final structures of the four MD simulations of FurE. The two gates are indicated by arrow heads: intracellular gate L4 between TMS4–TMS5 and extracellular gate L9 between TMS9-TMS10. Notice that the outer gate L9 bends covering the binding cavity at pH 5.0 and 6.8, while it remains in open position in the Ala 24–28 mutant. Notice also that the intracellular TMS5 segment shows a propensity to bend, opening the inner gate in the LID mutant, but less apparent in the other three simulated structures.

evidence of the flexibility of the LID and the stability of the hydrogen bonds observed in the model. Fundamental to successful MD simulation of a transmembrane protein is the accurate lipid bilayer composition chosen. Here, based on data available for the composition of fungal PM, the lipid bilayer used was composed of 40% phosphatidylcholine 16:1/18:1 (YOPC), 20% Ergosterol (ERG), and 40% phosphatidylinositol lipids (POPI). To specifically address the pH-dependent specificity of FurE, we selected different phosphatidylinositol lipids to emulate different pH environments. For the acidic pH (5.0), POPI lipid models were selected with overall charge −1 (not phosphorylated inositol). For the neutral pH (6.8), 20% POPI and 20% monophosphorylated POPI on position 4 or 5 of inositol with overall charge −3 were mixed (POPI14 or POPI15 equally distributed). Finally, for the basic pH (8.0), we have selected 20% POPI and 20% diphosphorylated POPI on position 4 and 5 of inositol (POPI24 or POPI25 equally distributed), with overall charge −4. In addition, we ran MD simulations of the FurE mutant version where residues 24–28 of the LID were Ala substituted, using the lipid bilayer simulation for neutral pH (6.8). FurE was embedded on each lipid bilayer and solvated by explicit water molecules (TIP3P), and 100 ns of simulation has been calculated in all four cases.

The MD simulations reveal that the N-terminus is highly mobile between residues 20–28, that is, the LID, while the part proximal to TMS1 (residues 30–40) has much less flexibility. The RMSD of the backbone depicted in Fig. 7A shows that in all cases, except at pH 5.0, the LID is flexible after the first 30-ns period of simulation. Figure 7B–E and Supplementary Video 1 illustrate the significant motion of the LID residues 20–28 and the rather fixed position of downstream residues 29–40, which remain at

proximity with mostly L8, but also L2 and L10. It is interesting to notice that although the LID mutant (Ala substituted 24–28) was simulated using the lipid bilayer for neutral pH (6.8), it displays different and more flexible dynamic behavior compared to the wild type, which exhibits only minor deviation from the initial structure for more than the first part of the calculation revisiting positions close to it for the rest of the simulated time. The highest RMSD is attained in the simulation at pH 8.0, reaching 15 Å for most of the calculated time period. This might be due to the higher number of interactions of Lys25 with lipid molecules (Supplementary Fig. 2A), in addition to a role of other positively charged residues, such as Lys188 and Arg360, attracted to PIP2 molecules due to the negative charge of the phosphorylated phosphatidylinositol (Supplementary Fig. 2B). The apparent stability of the segment of residues 29–40 was in good agreement with the experimentally defined structures of Mhp1. The comparison between the two crystal structures, outward-open (2jln) and inward-open (2 × 79), presented in Supplementary Fig. 3 shows that only the segment upstream from the small bend at $P15^{Mhp1}$ is re-oriented in the inward position, thus relaxing the interaction between LID and L8 as TMS8 is also slightly bent, similarly to what has been shown for LeuT [34]. Although there are important differences between Mhp1 and LeuT in the mechanism of substrate translocation, it appears that the interruption of the contact between the N-terminus and L8 is common in both cases. Our results suggest that FurE displays the tendency to follow a motion more similar to that observed in Mhp1.

To better visualize and further understand the specific motions of the different helices during the MD simulation, we have investigated (a) the RMSD of each individual helix, (b) the corresponding tilt compared to the *Z*-axis, and (c) the distance of each axis center to that of TMS2, which is the TMS with less motion (Supplementary Fig. 4). The calculations show that at all pHs and for the LID mutant, helices TMS4, 5, 9 and 10 have a higher propensity to bend, specifically at the loops L4 and L9. The RMSD from the initial position calculated during the MD simulation shows that all four TMSs move away from the starting structure between 2 to 5 Å (Supplementary Fig. 4A–D). Differences between the four simulations are more pronounced in the case of TMS5, where it seems that in case of simulation of wild-type FurE at pH 8.0 and for the LID mutant (pH 6.8), the deviations are larger than those of wild-type FurE at pH 5.0 and 6.8. Similarly, highest deviations of the initial value are observed for the tilt of the helices compared to the *Z*-axis observed in the case of TMS5, with the LID mutant tilting in the opposite direction compared to the three different simulations of pH (Supplementary Fig. 4E–H). Finally, when comparing the distance of the axis between the four TMSs 4, 5, 9 and 10 with TMS2, again the highest variation was observed in the case of TMS5, where the mutant displays the highest deviation from the initial value, while the pH 5.0 simulation remains almost stable (Supplementary Fig. 4I–L). Importantly, the specific tendency is clearer when comparing the TMS5 and TMS9 with the inward open structure of Mhp1. In Fig. 7F–G, the final structures of each one of the four MD calculations are superimposed together with the inward-open Mhp1 structure (2 × 79). In all four cases, TMS5 bends toward the inward conformation, with the simulation of pH 8.0 approaching closer to the open structure of Mhp1. In the extracellular interface, TMS9 shows the highest deviation, with the LID mutant tending to remain in the outward-open conformation, while at all pH simulations, L9 is bent, as also found with the Mhp1 inward-open structure.

Overall, MD simulations suggest that the N-terminal LID exhibits relatively high flexibility at the initial part of calculations, more pronounced in the case of pH 8.0 and in the LID mutant, mainly driven from the stronger coulombic interactions between positively charged amino acid residues and negatively charged lipids. These interactions mostly influence putative contacts with L8 and TMS9, as shown in Fig. 7F–G. The proximity of TMS9 to TMS4 appears to be the main reason of a concerted influence to TMS4 and TMS5. The main conclusion from the above MD calculations is that LID motions can influence, in a pH-dependent manner, both the exterior and interior gates and thereby the substrate translocation and transporter specificity. What is also notable is that when the LID motions are higher, as in the case of pH 8.0 or in the LID mutant, FurE acts as a promiscuous transporter recognizing all possible substrates. It becomes more specific for uracil and allantoin as shown from lower pH simulations performed with the wild-type protein.

Specific C-terminal elements are necessary for endocytosis, transport activity and substrate specificity

In Papadaki *et al*. [46], we showed that truncation of the 30 last residues of the FurE C-terminus (FurE-Δ498–528) has a dual effect; it blocks endocytosis and leads to a specificity change, in particular loss of uric acid transport. A block of endocytosis of FurE is also achieved when we replace the most distal two lysines in the C-tail (K521, K522) with arginine residues (Supplementary Fig. 5). This strongly suggests that block in endocytosis in FurE-ΔC30 is primarily due to the lack of these two lysines that apparently act as ubiquitin acceptor residues. To better define the limits of C-terminal segments that affect endocytosis *versus* substrate specificity, we performed systematic Ala replacements of the last 30 residues of the FurE C-tail (Fig. 8A).

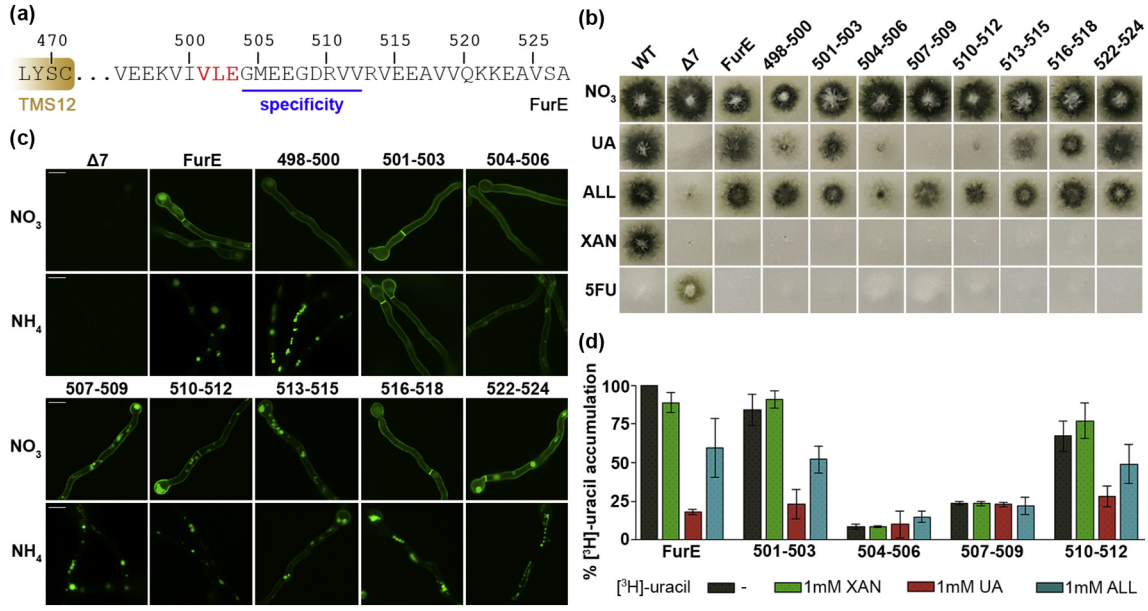

Fig. 8. Systematic mutational analysis of the C-terminus defines the limits of elements necessary for endocytosis, transport activity and substrate specificity. (A) Sequence of the cytosolic distal C-terminal region of FurE (495–527). The residues involved in endocytosis are highlighted in red, and the region involved in substrate specificity determination is underlined, as evidenced in panels B and C. (B) Growth tests of control strains and FurE mutants expressing triple Ala substitutions in the FurE C-terminal region. Each mutant is named after the position of residues replaced. Notice that mutants 504–506, 507–509 and 510–512 have totally lost the ability to grow on UA, while 513–515 has reduced growth on UA. Mutant 504–506 has also significantly reduced ability to grow on ALL and is partially resistant to 5FU, signifying that this mutant is a nearly loss-of-function mutant overall. Details are as in Fig. 1B. (C) Epifluorescence microscopy of the mutants shown in panel A. Notice that in the absence of an endocytic signal (NO_3 panel), all FurE mutants are normally localized in the PM. However, in mutants 501–503 and 504–506, FurE shows increased stability with no sign of steady-state vacuolar turnover, as in the wild-type FurE or the other mutants. This is in line with the observation that in these mutants, and particularly in 501–503, FurE is also resistant to NH_4^+-elicited endocytosis, suggesting that the sequence V-L-E is a primary element necessary for endocytosis. Finally, the fact that the following sequence G-M-E (504–506) is critical for the transport of all substrates (as shown in panel B) reveals that this element is absolutely essential for the transport mechanism of FurE per se. Scale bars represent 5 μm. (D) Accumulation of [^{3}H]-uracil in the simultaneous presence of excess (1 mM) of various substrates as indicated. Details are as in Fig. 2C. Standard deviation is depicted with error bars.

Figure 8B and C shows that triple Ala replacements in the C-terminus affect transport activity, specificity and endocytic turnover of FurE. Ala substitutions of 504–506, 507–509 and 510–512 abolished the ability for growth on uric acid. Mutations in 504–506 also had a strong reducing effect on growth on allantoin and led to partial resistance to 5FU, showing that the sequence G-M-E is absolutely essential for transport activity per se. Ala substitutions in 513–515 had a moderate effect on uric acid growth. Finally, Ala mutations in the distal C-tail (516–524) had no apparent effect on FurE function. These findings showed that the C-tail is critical for both transport activity (504–506) and specificity 507–512 (Fig. 8A). In respect to NH_4^+-elicited endocytosis, Ala mutations in 501–503 were sufficient to totally block endocytosis, similarly to deletion of the C30 segment. Partial abolishment of endocytosis was also observed with Ala mutations in 504–506 and 513–518, which might be due to an indirect effect on the topology of 501–503 (Fig. 8B).

We also performed radiolabel uracil uptake or competition assays for mutations 501–503, 504–506, 507–509 and 510–512, which seemed to define functional or specificity elements in FurE. Mutations 501–503 and 510–512 conserved 68%–80% of the wild-type FurE transport activity, but mutations 504–506 and 507–509 showed significantly reduced activities (~11%–20%; see gray bars in Fig. 8D). In competition assays, mutation 501–503 behaved similarly to the strain expressing wild-type FurE and reflected a significant (~75%) inhibition by excess uric acid (i.e., a high-affinity substrate), moderate (~39%) inhibition by allantoin (i.e., a low-affinity substrate), and no inhibition by xanthine (i.e., a non-substrate). Mutant 510–512 showed reduced inhibition by either uric acid or allantoin compared to wild-type FurE. Finally, mutations 504–506 and 507–509 showed practically no measurable binding of uric acid, allantoin or xanthine, which is in agreement with growth tests showing no or very little growth on these purines. Thus, direct uptake measurements

further confirmed that residues 504–512 are important for the function and specificity of FurE, while residues that affect endocytosis (501–503) are not critical for function or specificity.

Discussion

The importance of cytosolic termini in membrane trafficking processes has been well documented in several structurally, functionally and evolutionary distinct eukaryotic transporters, such as those specific for amino acids [8,15,18,50], glucose [4,5,14,26], carboxylic acids [3,13], L-ascorbic acid [38,58], nucleobases [27] or nucleosides [11,49]. In some cases, cytosolic termini are also known to affect the basic transport mechanism [7,14,19,31,40,42,51,56,57,64]. However, in no case, except FurE [46], have cytosolic termini been shown to control substrate *specificity* (for a recent review, see Ref. [44]). Here we provide new evidence and a mechanistic rationale on how cytosolic termini affect specificity through regulation of selective gating. First, using a systematic reverse genetic approach, we topologically and functionally defined the segments of the N- and C-termini that play distinct roles in trafficking, endocytosis or transport function per se. Subsequently, we show, based on unbiased genetic screens and dynamic modeling approaches that the N-terminus of FurE interacts with several internal loops and with the C-terminus, and we identify specific residues crucial for these interactions by systematic mutational analysis. Finally, we show, through extensive MD simulations that interactions of termini with internal loops are "allosterically" transmitted to the opening and closing of gates.

Interestingly, N- and C-terminal elements of FurE affected both endocytosis and transport specificity. A critical point in our study was to uncouple the role of distinct terminal elements in these two processes. Thus, endocytosis was found to require, in addition to K521 and K522 that act as ubiquitylation sites, a short C-terminal sequence M-E–E (residues 501–503) and elements within the distal part of the N-terminus (1–21). The need of both terminal segments of FurE for proper endocytic turnover, apparently via a mechanism that involves their dynamic cross-talk [46], helps to explain how specific conformational changes associated with the transition from an outward to an inward conformation are related with endocytic turnover [9,18]. In a simplified model, when the distal cytosolic termini interact closely with each other and other internal loops, the transporter is found in an outward-facing conformation, while when the interactions of termini and other loops becomes relaxed, the transporter is free to alternate in an inward-facing conformation, open to the cytosolic side. This in turn suggests that relaxation of the tight interaction of the N- and C-terminal regions associated with the inward-facing conformation produces a specific conformation more attractive for endocytic turnover. It seems reasonable to propose that N- and C-terminal sequences co-operatively and dynamically regulate the recruitment of the ubiquitylation machinery (e.g., accessibility of arrestin adaptors), which precedes endocytic turnover.

Delimiting the role of terminal elements in FurE endocytosis helped in defining the exact sequences in the two cytosolic termini that are crucial for determining substrate specificity, namely, residues 15–31 in the N-terminus and 504–512 in the C-terminus. While work from other groups has shown that cytosolic termini might be critical for overall transport activity, apparently through their effect on the alteration from an outward to an inward topology [7,19,31,42,51,56,57], this does not seem to be the case of FurE, where relevant terminal truncations or mutations affect specificity, rather than overall transport activity. This in turn suggests that specific terminal elements finely regulate the process of gating, rather than the basic alteration from outward to inward conformation.

The proposed interactions of the N-terminal region, and in particular of the LID, with specific internal loops provide a rationale on how the role of termini might be transmitted to the opening and closing of gates along the substrate translocating trajectory. More specifically, MD simulations provided evidence that the LID and consequently LID mutations affect, in pH-dependent manner, the relative topology of TMS9-TMS10 (outer gate) and TMS4–TMS5 (inner gate). It should be noted that in our simulations the influence of the charges on the lipid membrane was of crucial importance for approximation of different pHs. Experimental determination of the exact lipid composition of *A. nidulans* PM will be needed to validate our current approach.

Interestingly, FurE proved to function as a rather specific 5FU/uracil transporter at low pH, but as the pH increases, FurE becomes progressively more promiscuous, also transporting uric acid and allantoin, and eventually xanthine. Given that FurE versions carrying LID mutations mimic the specificity profile of the wild-type FurE at high pH, the relevant mutations seem to lead to loosening of gating, and thus to increased promiscuity in substrate selection. The relative MD analysis of the wild-type and mutant versions of FurE further supported the idea that stricter gating, which leads restricted specificity, is associated with tighter interactions of the cytosolic tails with internal loops. On the contrary, relaxed gating, which leads to transport of increased number of substrates, is associated with loosening of the tight interaction of tails with the main body of the transporter.

Materials and Methods

Media, strains and growth conditions

Standard complete (CM) and minimal media (MM) for *A. nidulans* growth were used. Media and supplemented auxotrophies were used at the concentrations given in http://www.fgsc.net. Glucose 1% (w/v) was used as carbon source. Ammonium tartrate (NH_4; 10 mM) or sodium nitrate (NO_3) was used as nitrogen source. Nucleobases and analogues were used at the following final concentrations: 5FU 100 μM, uric acid (UA) 0.5 mM, xanthine (XAN) and allantoin (ALL) 1 mM. All media and chemical reagents were obtained from Sigma-Aldrich (Life Science Chemilab SA, Hellas) or AppliChem (Bioline Scientific SA, Hellas). A *ΔfurD::riboB ΔfurA::riboB ΔfcyB::argB ΔazgA ΔuapA ΔuapC::AfpyrG ΔcntA::riboB pabaA1 pantoB100* mutant strain, named Δ7, was the recipient strain in transformations with plasmids carrying *fur* genes or alleles based on complementation of the pantothenic acid auxotrophy *pantoB100* [36]. The Δ7 strain has an intact endogenous FurE gene transporter, but this is very little expressed under standard conditions and thus does not contribute to detectable transport of its physiological substrates (UA, ALL) or to sensitivity in 5FU [37]. *A. nidulans* protoplast isolation and transformation was performed as previously described [32]. Growth tests were performed at 37 °C for 48 h, at pH 6.8 or at pH 5.0 and pH 8.0 where indicated.

Standard molecular biology manipulations and plasmid construction

Genomic DNA extraction from *A. nidulans* was performed as described in FGSC (http://www.fgsc.net). Plasmids, prepared in *Escherichia coli*, and DNA restriction or PCR fragments were purified from agarose 1% gels with the Nucleospin Plasmid Kit or Nucleospin ExtractII kit, according to the manufacturer's instructions (Macherey–Nagel, Lab Supplies Scientific SA, Hellas). Standard PCR reactions were performed using KAPATaq DNA polymerase (Kapa Biosystems). PCR products used for cloning, sequencing and re-introduction by transformation in *A. nidulans* were amplified by a high-fidelity KAPA HiFi HotStart Ready Mix (Kapa Biosystems) polymerase. DNA sequences were determined by VBC-Genomics (Vienna, Austria). Site-directed mutagenesis was carried out according to the instructions accompanying the Quik-Change® Site-Directed Mutagenesis Kit (Agilent Technologies, Stratagene). The principal vector used for most *A. nidulans* mutants is a modified pGEM-T-easy vector carrying a version of the *gpdA* promoter, the *trpC* 3′ termination region and the panB selection marker [37]. Mutations and segment truncations in Fur transporters were constructed by oligonucleotide-directed mutagenesis or appropriate forward and reverse primers (Table S2). Transformants arising from single copy integration events with intact Fur ORFs were identified by Southern and PCR analysis.

Uptake assays

Kinetic analysis of Fur transporters activity was measured by estimating uptake rates of [^{3}H]-uracil uptake (40 Ci mmol^{-1}, Moravek Biochemicals, CA, USA), as previously described by Krypotou and Diallinas [36]. In brief, [^{3}H]-uracil uptake was assayed in *A. nidulans* conidiospores germinating for 4 h at 37 °C, at 140 rpm, in liquid MM (pH 6.8). Initial velocities were measured on 10^7 conidiospores/100 μL by incubation with concentrations of 0.2–2.0 μM of [^{3}H]-uracil at 37 °C. For the competition experiments, initial uptake rates of [^{3}H]-uracil were measured in the simultaneous presence of excess (1 mM) of various putative substrates as indicated. The time of incubation was defined through time-course experiments at 4 min, when the transporter showed linear increased activity. All transport assays were carried out at least in two independent experiments and the measurements in triplicate. Standard deviation was $<$20%. Results were analyzed in GraphPad Prism software.

Isolation and characterization of suppressor mutations

Suppressor mutations of 10^9 conidiospores of the strain S15A/L16A were obtained after 3-min 45-s exposure at a standard distance of 20 cm from an Osram HNS30 UV-B/C lamp and subsequent selection of colonies capable of growing on MM containing uric acid as sole nitrogen source, at 25 °C. Spores from positive colonies were collected after 6–8 days and further isolated on the same selective medium that was used to obtain the original colonies. Genomic DNA from 24 purified colonies was isolated and the ORF of FurE was amplified and sequenced. In all cases, the amplified fragments contained a new mutation.

Epifluorescence microscopy

Samples for standard epifluorescence microscopy were prepared as previously described [16,27]. In brief, sterile 35-mm l-dishes with a glass bottom (Ibidi, Germany) containing liquid minimal media supplemented with $NaNO_3$ and 0.1% glucose were inoculated from a spore solution and incubated for 18 h at 25 °C. The samples were observed on an Axioplan Zeiss phase contrast epifluorescent microscope, and the resulting images were acquired with

a Zeiss-MRC5 digital camera using the AxioVs40 V4.40.0 software. Image processing and contrast adjustment were made using the ZEN 2012 software, while further processing of the TIFF files was made using Adobe Photoshop CS3 software for brightness adjustment, rotation and alignment.

Homology modeling

The construction of a structural model of FurE was based on the crystal structure of the Mhp1 benzylhydantoin permease from *Microbacterium liquefaciens* in the outward-open structure (PDB entry 2JLN). We utilized as starting alignment the one already described by our group [37] and optimized based on mutation analysis data (Supplementary Fig. 1). The final model was built using PRIME software with an energy-based algorithm [23]. A loop refinement routine was also implemented.

Molecular dynamics

FurE was inserted into a lipid bilayer using the CHARMM-GUI tool [63]. The resulting system was explicitly solvated using the TIP3P water model [24] and neutralized by the addition of Na^+ and Cl^- counter ions at concentration of 0.15 M. For the acidic pH (5.0) emulation, the lipid bilayer used was composed of 40% phosphatidylcholine 16:1/18:1 (YOPC), 20% Ergosterol (ERG) and 40% POPI lipid models, which were selected with an overall charge −1 (not phosphorylated inositol). For the neutral pH (6.8) emulation, the lipid bilayer used was composed of 40% phosphatidylcholine 16:1/18:1 (YOPC), 20% Ergosterol (ERG), and 20% POPI and 20% monophosphorilated POPI on position 4 or 5 of inositol (POPI14 or POPI15 was equally distributed), with an overall charge of −3. Finally, for the basic pH (8.0) emulation, the lipid bilayer used was composed of 40% phosphatidylcholine 16:1/18:1 (YOPC), 20% Ergosterol (ERG), 20% POPI and 20% di-phosphorylated POPI on position 4 and 5 of inositol (POPI24 or POPI25 was equally distributed), with an overall charge of −4. For the FurE LID mutant (24–28 Ala substitution), we utilized the pH 6.8 lipid bilayer emulation described above. Starting from wild-type FurE, on CHARMM-GUI's initial step "PDB Manipulation Options," we mutated residues 24–28 to alanines. In all cased, FurE was embedded on each lipid bilayer and solvated by explicit water molecules (TIP3P). The N-terminal residue (Ala20) was methylated and the C-terminus residue (Glu507) was amidated. All MD simulations were performed with GROMACS 2018 [1] using the all-atom force-field CHARMM36 [20]. Periodic boundary conditions were used. Long-range electrostatic interactions were treated with Particle Mesh Ewald method. Non-bonded interactions were described with a Lennard–Jones potential with a cut-off distance of 1 nm, and an integration step of 2 fs was implemented. The system was progressively minimized and equilibrated using the GROMACS input scripts generated by CHARMM-GUI, and the temperature and pressure were held at 303.15 K and 1 bar, respectively [39]. The resulting equilibrated structures were then used as an initial condition for the production runs of 100 ns, with all the constraints turned off. Production runs were subsequently analyzed using GROMACS tools, and all images and videos were prepared using VMD software [21].

Supplementary data to this article can be found online at https://doi.org/10.1016/j.jmb.2019.07.013.

Acknowledgments

We are grateful to Prof. Richard Naftalin for text corrections and scientific comment. This work was supported by a "Stavros S. Niarchos Foundation" grant and by computational time granted from the Greek Research & Technology Network in the National HPC facility—ARIS—under project NCS1_Mechanism (pr006040).

Author Contributions: G.F.P. performed all genetic and molecular experiments. A.Z., G.L. and E.M. performed the *in silico* analysis and the molecular dynamics, and analyzed results. E.M. wrote parts of the article. G.D. conceived and planned experiments analyzed results and wrote the article.

Conflict of Interest: The authors declare that they have no conflict of interest.

Received 3 April 2019;
Received in revised form 4 July 2019;
Accepted 4 July 2019
Available online 12 July 2019

Keywords:
Aspergillus nidulans;
fungi;
transport;
folding;
membrane lipids!

Abbreviations used:
NCS1, nucleobase cation symporter 1; TMS, transmembrane α-helical segment; MD, molecular dynamics; LID, loop interacting domain; 5FU, 5-fluorouracil.

References

[1] M.J. Abraham, T. Murtola, R. Schulz, S. Páll, J.C. Smith, B. Hess, E. Lindahl, GROMACS: high performance molecular

simulations through multi-level parallelism from laptops to supercomputers, SoftwareX 1–2 (2015) 19–25.
[2] J.L. Adelman, A.L. Dale, M.C. Zwier, D. Bhatt, L.T. Chong, D. M. Zuckerman, M. Grabe, Simulations of the alternating access mechanism of the sodium symporter Mhp1, Biophys. J. 101 (2011) 2399–2407.
[3] Becuwe M, Léon S (2014) Integrated control of transporter endocytosis and recycling by the arrestin-related protein Rod1 and the ubiquitin ligase Rsp5. *Elife* 3.
[4] P.D. Brewer, E.N. Habtemichael, I. Romenskaia, C.C. Mastick, A.C. Coster, Insulin-regulated Glut4 translocation: membrane protein trafficking with six distinctive steps, J. Biol. Chem. 289 (2014) 17280–17298.
[5] F.M. Brodsky, Diversity of clathrin function: new tricks for an old protein, Annu. Rev. Cell Dev. Biol. 28 (2012) 309–336.
[6] A.N. Calabrese, S.M. Jackson, L.N. Jones, O. Beckstein, F. Heinkel, J. Gsponer, D. Sharples, M. Sans, M. Kokkinidou, A. R. Pearson, S.E. Radford, A.E. Ashcroft, P.J.F. Henderson, Topological dissection of the membrane transport protein Mhp1 derived from cysteine accessibility and mass spectrometry, Anal. Chem. 89 (2017) 8844–8852.
[7] M.H. Cheng, I. Bahar, Complete mapping of substrate translocation highlights the role of LeuT N-terminal segment in regulating transport cycle, PLoS Comput. Biol. 10 (2014), e1003879.
[8] M. Crapeau, A. Merhi, B. André, Stress conditions promote yeast Gap1 permease ubiquitylation and down-regulation via the arrestin-like Bul and Aly proteins, J. Biol. Chem. 289 (2014) 22103–22116.
[9] G. Diallinas, Dissection of transporter function: from genetics to structure, Trends Genet. 32 (2016) 576–590.
[10] D. Drew, O. Boudker, Shared molecular mechanisms of membrane transporters, Annu. Rev. Biochem. 85 (2016) 543–572.
[11] E. Errasti-Murugarren, F.J. Casado, M. Pastor-Anglada, Different N-terminal motifs determine plasma membrane targeting of the human concentrative nucleoside transporter 3 in polarized and nonpolarized cells, Mol. Pharmacol. 78 (2010) 795–803.
[12] L.R. Forrest, G. Rudnick, The rocking bundle: a mechanism for ion-coupled solute flux by symmetrical transporters, Physiology (Bethesda) 24 (2009) 377–386.
[13] S. Fujita, D. Sato, H. Kasai, M. Ohashi, S. Tsukue, Y. Takekoshi, K. Gomi, T. Shintani, The C-terminal region of the yeast monocarboxylate transporter Jen1 acts as a glucose signal-responding degron recognized by the α-arrestin Rod1, J. Biol. Chem. 293 (2018) 10926–10936.
[14] T. Galochkina, M. Ng Fuk Chong, L. Challali, S. Abbar, C. Etchebest, New insights into GluT1 mechanics during glucose transfer, Sci. Rep. 9 (1) (2019) 998.
[15] K. Ghaddar, A. Merhi, E. Saliba, E.M. Krammer, M. Prévost, B. André, Substrate-induced ubiquitylation and endocytosis of yeast amino acid permeases, Mol. Cell. Biol. 34 (2014) 4447–4463.
[16] C. Gournas, S. Amillis, A. Vlanti, G. Diallinas, Transport-dependent endocytosis and turnover of a uric acid-xanthine permease, Mol. Microbiol. 75 (2010) 246–260.
[18] C. Gournas, M. Prévost, E.M. Krammer, B. André, Function and regulation of fungal amino acid transporters: insights from predicted structure, Adv. Exp. Med. Biol. 892 (2016) 69–106.
[19] B. Guptaroy, M. Zhang, E. Bowton, F. Binda, L. Shi, H. Weinstein, A. Galli, J.A. Javitch, R.R. Neubig, M.E. Gnegy, A juxtamembrane mutation in the N terminus of the dopamine transporter induces preference for an inward-facing conformation, Mol. Pharmacol. 75 (2009) 514–524.
[20] J. Huang, A.D. MacKerell Jr., CHARMM36 all-atom additive protein force field: validation based on comparison to NMR data, J. Comput. Chem. 34 (2013) 2135–2145.
[21] W. Humphrey, A. Dalke, K. Schulten, VMD—visual molecular dynamics, J Molec Graphics 14 (1996) 33–38.
[22] H. Ilgü, J.M. Jeckelmann, V. Gapsys, Z. Ucurum, B.L. de Groot, D. Fotiadis, Insights into the molecular basis for substrate binding and specificity of the wild-type L-arginine/agmatine antiporter AdiC, Proc. Natl. Acad. Sci. U. S. A. 113 (2016) 10358–10363.
[23] Jacobson MP, Pincus DL, Rapp CS, Day TJ, Honig B, Shaw DE, Friesner RA (2004) A hierarchical approach to all-atom protein loop prediction. *Proteins* 55: 351-367
[24] W.L. Jorgensen, J. Chandrasekhar, J.D. Madura, R.W. Impey, M.L. Klein, Comparison of simple potential functions for simulating liquid water, J. Chem. Phys. 79 (1983) 926–935.
[25] H.R. Kaback, I. Smirnova, V. Kasho, Y. Nie, Y. Zhou, The alternating access transport mechanism in LacY, J. Membr. Biol. 239 (2011) 85–93.
[26] K.V. Kandror, P.F. Pilch, The sugar is sIRVed: sorting Glut4 and its fellow travelers, Traffic 12 (2011) 665–671.
[27] M. Karachaliou, S. Amillis, M. Evangelinos, A.C. Kokotos, V. Yalelis, G. Diallinas, The arrestin-like protein ArtA is essential for ubiquitination and endocytosis of the UapA transporter in response to both broad-range and specific signals, Mol. Microbiol. 88 (2013) 301–317.
[28] K. Kazmier, D.P. Claxton, H.S. Mchaourab, Alternating access mechanisms of LeuT-fold transporters: trailblazing towards the promised energy landscapes, Curr. Opin. Struct. Biol. 45 (2017) 100–108.
[29] K. Kazmier, S. Sharma, S.M. Islam, B. Roux, H.S. Mchaourab, Conformational cycle and ion-coupling mechanism of the Na^+/hydantoin transporter Mhp1, Proc. Natl. Acad. Sci. U. S. A. 111 (2014) 14752–14757.
[30] J.M. Keener, M. Babst, Quality control and substrate-dependent downregulation of the nutrient transporter Fur4, Traffic 14 (2013) 412–427.
[31] G. Khelashvili, M. Doktorova, M.A. Sahai, N. Johner, L. Shi, H. Weinstein, Computational modeling of the N-terminus of the human dopamine transporter and its interaction with PIP2-containing membranes, Proteins 83 (2015) 952–969.
[32] M. Koukaki, E. Giannoutsou, A. Karagouni, G. Diallinas, A novel improved method for *Aspergillus nidulans* transformation, J. Microbiol. Methods 55 (2003) 687–695.
[33] H. Krishnamurthy, C.L. Piscitelli, E. Gouaux, Unlocking the molecular secrets of sodium-coupled transporters, Nature 459 (2009) 347–355.
[34] H. Krishnamurthy, E. Gouaux, X-ray structures of LeuT in substrate-free outward-open and apo inward-open states, Nature 481 (2012) 469–474.
[35] E. Krypotou, V. Kosti, S. Amillis, V. Myrianthopoulos, E. Mikros, G. Diallinas, Modeling, substrate docking, and mutational analysis identify residues essential for the function and specificity of a eukaryotic purine-cytosine NCS1 transporter, J. Biol. Chem. 287 (2012) 36792–36803.
[36] E. Krypotou, G. Diallinas, Transport assays in filamentous fungi: kinetic characterization of the UapC purine transporter of *Aspergillus nidulans*, Fungal Genet. Biol. 63 (2014) 1–8.
[37] E. Krypotou, T. Evangelidis, J. Bobonis, A.A. Pittis, T. Gabaldón, C. Scazzocchio, E. Mikros, G. Diallinas, Origin,

diversification and substrate specificity in the family of NCS1/FUR transporters, Mol. Microbiol. 96 (2015) 927–950.
[38] S.M. Kuo, L.Y. Wang, S. Yu, C.E. Campbell, S.A. Valiyaparambil, M. Rance, K.M. Blumenthal, The N-terminal basolateral targeting signal unlikely acts alone in the differential trafficking of membrane transporters in MDCK cells, Biochemistry 52 (2013) 5103–5116.
[39] J. Lee, X. Cheng, J.M. Swails, M.S. Yeom, P.K. Eastman, J. A. Lemkul, S. Wei, J. Buckner, J.C. Jeong, Y. Qi, S. Jo, V.S. Pande, D.A. Case, C.L. Brooks 3rd, A.D. MacKerell Jr., J.B. Klauda, W. Im, CHARMM-GUI input generator for NAMD, GROMACS, AMBER, OpenMM, and CHARMM/OpenMM simulations using the CHARMM36 additive force field, J. Chem. Theory Comput. 12 (2016) 405–413.
[40] D. Ma, P. Lu, Y. Shi, Substrate selectivity of the acid-activated glutamate/γ-aminobutyric acid (GABA) antiporter GadC from *Escherichia coli*, J. Biol. Chem. 288 (2013) 15148–15153.
[41] P. Ma, S.G. Patching, E. Ivanova, J.M. Baldwin, D. Sharples, S.A. Baldwin, P.J. Henderson, Allantoin transport protein, PucI, from *Bacillus subtilis*: evolutionary relationships, amplified expression, activity and specificity, Microbiology 162 (2016) 823–836.
[42] L. Malinauskaite, M. Quick, L. Reinhard, J.A. Lyons, H. Yano, J.A. Javitch, P. Nissen, A mechanism for intracellular release of Na^+ by neurotransmitter/sodium symporters, Nat. Struct. Mol. Biol. 21 (2014) 1006–1012.
[44] E. Mikros, G. Diallinas, Tales of tails in transporters, Open Biol. 9 (6) (2019) 190083.
[45] A. Pantazopoulou, N.D. Lemuh, D.G. Hatzinikolaou, C. Drevet, G. Cecchetto, C. Scazzocchio, G. Diallinas, Differential physiological and developmental expression of the UapA and AzgA purine transporters in *Aspergillus nidulans*, Fungal Genet. Biol. 44 (2007) 627–640.
[46] G.F. Papadaki, S. Amillis, G. Diallinas, Substrate specificity of the FurE transporter is determined by cytoplasmic terminal domain interactions, Genetics 207 (2017) 1387–1400.
[47] I. Papageorgiou, C. Gournas, A. Vlanti, S. Amillis, A. Pantazopoulou, G. Diallinas, Specific interdomain synergy in the UapA transporter determines its unique specificity for uric acid among NAT carriers, J. Mol. Biol. 382 (2008) 1121–1135.
[48] S.G. Patching, Recent developments in nucleobase cation symporter-1 (NCS1) family transport proteins from bacteria, archaea, fungi and plants, J. Biosci. 43 (2018) 797–815.
[49] I. Pinilla-Macua, F.J. Casado, M. Pastor-Anglada, Structural determinants for rCNT2 sorting to the plasma membrane of polarized and non-polarized cells, Biochem. J. 442 (2012) 517–525.
[50] D. Popov-Čeleketić, F. Bianchi, S.J. Ruiz, F. Meutiawati, B. Poolman, A plasma membrane association module in yeast amino acid transporters, J. Biol. Chem. 291 (2016) 16024–16037.
[51] A.M. Razavi, G. Khelashvili, H. Weinstein, How structural elements evolving from bacterial to human SLC6 transporters enabled new functional properties, BMC Biol. 16 (2018) 31.
[52] Y. Shi, Common folds and transport mechanisms of secondary active transporters, Annu. Rev. Biophys. 42 (2013) 51–72.
[53] T. Shimamura, S. Weyand, O. Beckstein, N.G. Rutherford, J. M. Hadden, D. Sharples, M.S. Sansom, S. Iwata, P.J. Henderson, A.D. Cameron, Molecular basis of alternating access membrane transport by the sodium-hydantoin transporter Mhp1, Science 328 (2010) 470–473.
[54] K.J. Simmons, S.M. Jackson, F. Brueckner, S.G. Patching, O. Beckstein, E. Ivanova, T. Geng, S. Weyand, D. Drew, J. Lanigan, D.J. Sharples, M.S. Sansom, S. Iwata, C.W. Fishwick, A.P. Johnson, A.D. Cameron, P.J. Henderson, Molecular mechanism of ligand recognition by membrane transport protein, Mhp1, EMBO J. 33 (2014) 1831–1844.
[55] G. Sioupouli, G. Lambrinidis, E. Mikros, S. Amillis, G. Diallinas, Cryptic purine transporters in *Aspergillus nidulans* reveal the role of specific residues in the evolution of specificity in the NCS1 family, Mol. Microbiol. 103 (2017) 319–332.
[56] S. Sucic, S. Dallinger, B. Zdrazil, R. Weissensteiner, T.N. Jørgensen, M. Holy, O. Kudlacek, S. Seidel, J.H. Cha, U. Gether, A.H. Newman, G.F. Ecker, M. Freissmuth, H.H. Sitte, The N terminus of monoamine transporters is a lever required for the action of amphetamines, J. Biol. Chem. 285 (2010) 10924–10938.
[57] C.G. Sweeney, B.P. Tremblay, T. Stockner, H.H. Sitte, H.E. Melikian, Dopamine transporter amino and carboxyl termini synergistically contribute to substrate and inhibitor affinities, J. Biol. Chem. 292 (2017) 1302–1309.
[58] S. Varma, K. Sobey, C.E. Campbell, S.M. Kuo, Hierarchal contribution of N- and C-terminal sequences to the differential localization of homologous sodium-dependent vitamin C transporters, SVCT1 and SVCT2, in epithelial cells, Biochemistry 48 (2009) 2969–2980.
[59] Å. Västermark, M.H. Saier Jr., Evolutionary relationship between 5 + 5 and 7 + 7 inverted repeat folds within the amino acid-polyamine-organocation superfamily, Proteins 82 (2014) 336–346.
[60] A. Vlanti, G. Diallinas, The *Aspergillus nidulans* FcyB cytosine–purine scavenger is highly expressed during germination and in reproductive compartments and is downregulated by endocytosis, Mol. Microbiol. 68 (2008) 959–977.
[61] S. Weyand, T. Shimamura, S. Yajima, S. Suzuki, O. Mirza, K. Krusong, E.P. Carpenter, N.G. Rutherford, J.M. Hadden, J. O'Reilly, P. Ma, M. Saidijam, S.G. Patching, R.J. Hope, H.T. Norbertczak, P.C. Roach, S. Iwata, P.J. Henderson, A.D. Cameron, Structure and molecular mechanism of a nucleobase-cation-symport-1 family transporter, Science 322 (2008) 709–713.
[62] F.H. Wong, J.S. Chen, V. Reddy, J.L. Day, M.A. Shlykov, S. T. Wakabayashi, M.H. Saier Jr., The amino acid-polyamine-organocation superfamily, J. Mol. Microbiol. Biotechnol. 22 (2012) 105–113.
[63] E.L. Wu, X. Cheng, S. Jo, H. Rui, K.C. Song, E.M. Dávila-Contreras, Y. Qi, J. Lee, V. Monje-Galvan, R.M. Venable, J. B. Klauda, W. Im, CHARMM-GUI membrane builder toward realistic biological membrane simulations, J. Comput. Chem. 35 (2014) 1997–2004.
[64] J.V. Busto, A. Elting, D. Haase, F. Spira, J. Kuhlman, M. Schäfer-Herte, R. Wedlich-Söldner, Lateral plasma membrane compartmentalization links protein function and turnover, EMBO J. 37 (16) (2018 Aug 15)https://doi.org/10.15252/embj.201899473.